Res Intell Manuf Assem, 2026, 5(1): 340-359
DOI: 10.25082/RIMA.2026.01.004

RESEARCH ARTICLE

Computational and Experimental Investigation of Peel and Shear Stress Distribution in Adhesively Bonded Hybrid Sisal-Glass Reinforced HDPE Composite for Automobile Side Body Panel

Samuel Tesfaye Molla[1*] **Assefa Asmare Tsegaw**[1] **Teshome Mulatie Bogal**[1] **Addisu Negash Ali**[1] **Asmamaw Tegegne Abebe**[2]

[1] Department of Mechanical Engineering, Faculty of Mechanical and Industrial Engineering, Bahir Dar Institute of Technology, Bahir Dar University, Bahir Dar, Ethiopia
[2] Department of Manufacturing Technology, Faculty of Mechanical Technology, Federal TVTI, Addis Abeba, Ethiopia

Correspondence to: Samuel Tesfaye Molla, Department of Mechanical Engineering, Faculty of Mechanical and Industrial Engineering, Bahir Dar Institute of Technology, Bahir Dar University, Bahir Dar,Ethiopia; Email: Samitommy928556@gmail.com

Received: December 7, 2025;
Accepted: April 6, 2026;
Published: April 9, 2026.

Citation: Molla ST, Tsegaw AA, Bogale TM, et al. Computational and Experimental Investigation of Peel and Shear Stress Distribution in Adhesively Bonded Hybrid Sisal-Glass Reinforced HDPE Composite for Automobile Side Body Panel. *Res Intell Manuf Assem*, 2026, **5**(1): 340-359.
https://doi.org/10.25082/RIMA.2026.01.004

Abstract: This study presents an integrated computational and experimental study of peel and shear stress distributions in adhesively bonded single-side strap joints (ABSSSJ). These joints comprise a hybrid sisal-glass reinforced HDPE lower adherend and a steel upper adherend for automobile side body panel applications. The study combined fabrication and mechanical (tensile and lap-shear) testing of hybrid composites with different fiber ratios and stacking sequences; parametric Cohesive Zone Model (CZM) based finite-element simulations in ANSYS; and an analytical variational-method (VM) solution for interfacial stress functions to cross-validate numerical predictions. Adhesive properties (modulus 1.85–6.0 GPa), adhesive thickness (0.2–1.0 mm) and cohesive fracture toughness (G_{IC} = 0.25–1.0 kJ·m^{-2}) were varied. Environmental conditioning (moisture exposure 2–10 hr and Temperature 25–45°C) was included to assess durability effects. Key quantitative findings include that peak peel stress consistently occurs at the free edge of the overlap, while shear stress concentrates at the overlap ends. Increasing adhesive thickness from 0.2 to 1.0 mm reduced the peak peel stress ($\sim$12.3 $\rightarrow$ 8.7 MPa, $\approx$ 29% reduction) while producing modest increases in shear strain. The optimal joint performance occurred at an adhesive thickness $\approx$ 0.5 mm and $G_{IC} \approx$ 0.75 kJ·m^{-2}. The experimentally measured maximum shear strength of ABSSSJ reached 18.4 MPa (for 0.5 mm adhesive), and the tensile strength for the best stacking sequence (G–S–G) was 62.3 MPa. The CZM–FEM and VM predictions agreed closely with experimental results (deviation $\leq$ 8%), demonstrating the predictive capability of the combined approach. Moisture and elevated temperature degraded cohesive stiffness and increased the peel stress by 8–15%, underscoring the importance of accounting for environmental effects in design. These results advance both the mechanistic understanding and engineering readiness of recyclable, natural–synthetic hybrid composites for lightweight automotive structures.

Keywords: computational modeling, adhesively bonded joints, peel and shear stress distribution, cohesive zone modeling, finite element analysis

1 Introduction

The increasing demand for lightweight, sustainable, and high-performance materials in the automotive industry has intensified research into advanced bonding technologies and natural-fiber composites. Adhesively bonded joints (ABJ) are preferred over conventional mechanical fasteners because they can join dissimilar materials, reduce stress concentrations, distribute load uniformly, and improve corrosion resistance [1, 2]. Among joint configurations, the adhesively bonded single-sided strap joint (ABSSSJ) is widely used for its structural simplicity, manufacturability, and effective load transfer in automotive structures. Hybrid composites that combine natural and synthetic fibers have also gained attention. In particular, sisal–glass reinforced high-density polyethylene (HDPE) composites offer a favorable balance of mechanical performance, cost efficiency, and environmental sustainability [3–5]. These hybrid materials leverage the biodegradability and low cost of sisal fibers alongside the stiffness and strength of glass fibers, making them promising for semi-structural automotive components such as side-body panels. However, the performance of such ABJs is governed by the peel and shear stress distribution in the adhesive layer; uneven stresses often lead to premature debonding or adhesive/cohesive

failure [6–10]. Numerous studies have examined how parameters like adhesive thickness, overlap geometry, adherend stiffness, and fiber orientation affect stress concentrations and joint durability [11–14]. Meanwhile, cohesive zone models (CZM) implemented in finite-element analysis have proven effective at predicting damage initiation and progressive debonding in adhesive joints, yielding insights into crack propagation under mixed-mode loading [13–16]. Despite these advances, gaps remain. There are few studies that systematically combine experimental validation with CZM-based simulations for hybrid natural–synthetic composite joints. The sisal–glass/HDPE system poses additional challenges: sisal fibers are hydrophilic and anisotropic (leading to moisture sensitivity and property variability), while glass fibers increase stiffness but can cause stress mismatches at the adhesive–adherend interface [17, 18].

The purpose of this study is to investigate the peel and shear stress distribution in adhesively bonded steel–to–hybrid sisal–glass/HDPE joints using an integrated computational–experimental approach. We quantify how adhesive properties, overlap geometry, and composite architecture influence interfacial stress evolution and failure initiation in joints intended for automotive side-body panels. Although existing literature provides insights into natural-fiber composites [19, 20] and adhesive joint modeling [21, 22], three key limitations persist: First, most studies focus on either natural-fiber or synthetic-fiber composites alone, with limited work on steel bonded to hybrid sisal–glass/HDPE. Second, the application of CZM for predicting combined peel and shear stress distribution and full debonding in hybrid composite joints is scarce. Third, validated FEM frameworks that integrate cohesive modeling, orthotropic composite behavior, and experimental peel/shear testing in automotive joint configurations are largely absent. No prior work has integrated CZM, anisotropic composite modeling, and experimental peel/shear tests for such hybrid joints. Thus, a comprehensive computational–experimental framework is needed to fill this gap. To address these gaps, the present study combines a variational analytical method, CZM-based FEM, and experimental testing to assess peel and shear stress distributions in ABSSSJ configurations for automotive side panels. This research is significant in three ways. First, from the perspective of lightweight design, hybrid sisal–glass/HDPE composites offer low density, high impact strength, and corrosion resistance – critical properties for side-body panels. Understanding adhesive peel and shear stresses contributes directly to developing lighter, stronger bonded components. Second, in terms of structural integrity, peel and shear stresses govern failure initiation in bonded joints; accurate prediction via CZM–FEM (validated by experiments) enables better joint design, enhanced reliability, and reduced prototyping costs. Third, the study supports sustainable materials: sisal is abundantly available in Ethiopia and other regions, and hybridizing it with glass improves performance while preserving eco-friendliness [23]. These factors underscore both the scientific relevance and industrial applicability of our work.

The primary objective of this research is to analyze and compare peel and shear stress behavior in bonded hybrid sisal–glass/HDPE joints using analytical (variational), experimental, and CZM–FEM methods. We also examine how adhesive thickness, overlap dimensions, fiber orientation, and stacking sequence affect stress localization and failure mechanisms. Critical regions prone to crack initiation will be identified, and design recommendations will be proposed to improve the strength and integrity of adhesively bonded side-body panel joints.

Novelty Statement: To our knowledge, this is the first comprehensive study to integrate analytical variational methods, cohesive-zone finite-element modeling, and experimental validation for steel–sisal/glass-HDPE composite adhesive joints under mixed-mode loading, specifically addressing the identified literature gap in hybrid automotive composite joints.

2 Methodology

2.1 Overview of Methodology

The methodology adopted in this study focuses on the comparative investigation of peel and shear stress distributions, mechanical strength, and debonding behavior of adhesively bonded joints (ABJs) fabricated from hybrid sisal–glass reinforced HDPE composites and steel, with specific application to automobile side body panels. A combined computational and experimental approach was employed to ensure robust analysis and validation. The investigation integrates cohesive zone model (CZM)–based finite element method (FEM) simulations, analytical modeling using the variational method (VM), and experimental mechanical testing. Peel and shear stress distributions obtained from numerical simulations were validated against experimental observations to assess predictive accuracy. The methodology was designed to systematically evaluate the influence of key parameters, including adhesive thickness (AT), adhesive elastic

modulus (E), cohesive fracture toughness (G_{IC}), overlap dimensions (bond length, BL, and overlap width, OW), moisture exposure, temperature, fiber-to-matrix weight ratio, and surface finish characterized by sand grit number, on the performance of adhesively bonded single-side strap joints (ABSSSJ).

2.2 Computational Methods

2.2.1 Cohesive Zone Model (CZM) Based Finite Element Modeling (FEM)

CZM Based FEM was employed to simulate the mechanical response and progressive debonding behavior of the adhesively bonded joints and to analyze the shear stress distributions within the adhesive layer. The cohesive zone approach enables accurate representation of traction–separation behavior and damage evolution at the adhesive–adherend interface. A bilinear traction–separation law was used to define the adhesive behavior:

$$t = K\delta, \quad (\delta \leq \delta_0) \tag{1}$$

$$G_c = \int t \, \mathrm{d} \tag{2}$$

Where: t: traction stress, δ: separation displacement, K: interface stiffness, G_c: fracture energy.

This formulation is widely accepted for modeling adhesive fracture, and damage begins when the combinations of normal and shear stress tractions reaches their critical strengths. After initiation, the interface softens linearly until complete failure, with energy dissipations equal to G_{IC} and G_{IIC} [25].The numerical models were developed using ANSYS software. The ABSSSJ geometry was constructed to represent the actual joint configuration used in experimental testing (Figure 1). The lower adherend was modeled as a hybrid sisal–glass reinforced HDPE composite, while the upper adherend was modeled as steel. The composite adherend was represented using orthotropic shell elements (Shell181) to capture anisotropic material behavior arising from fiber orientation and stacking sequence. The steel adherend was modeled using isotropic plane strain elements (PLANE182). The adhesive layer was discretized using cohesive interface elements (INTER202), which allow simulation of damage initiation and propagation based on traction–separation laws. A refined mesh was applied in the adhesive layer and interfacial regions to ensure accurate stress resolution and convergence during debonding analysis. Mesh sensitivity studies were conducted to confirm numerical stability and accuracy of the predicted stress fields. Material properties, cohesive parameters, and boundary conditions were defined consistently with experimental conditions and analytical assumptions. Peel and shear stresses were extracted along the adhesive mid-plane and overlap length for comparative analysis with variational and experimental results.

2.2.2 Materials and Material Properties

The materials used in this study include a hybrid sisal–glass reinforced HDPE composite, a structural adhesive, and steel adherends. Material properties were defined based on experimental measurements and relevant literature and are summarized in Tables 1 and 2.

The hybrid composite properties include fiber-to-matrix weight ratio, fiber orientation [0/+45/90/-45/0][0/+45/90/-45/0][0/+45/90/-45/0], stacking sequence [S–G–G][S–G–G][S–G–G] and [G–S–G][G–S–G][G–S–G], as well as overlap length and overlap width of the lower adherend. These parameters were selected to represent realistic configurations for automobile side body panel applications. For the adhesive layer, variations in elastic modulus (E), adhesive thickness (AT), and cohesive fracture toughness (G_{IC}) were considered to evaluate their influence on stress distribution and debonding behavior. The steel adherend was modeled as an isotropic material, characterized by Young's modulus and Poisson's ratio, as listed in Table 2.

2.2.3 Boundary Conditions and Loading

Boundary conditions were defined to replicate the experimental shear and tensile testing conditions of the adhesively bonded single-side strap joint (ABSSSJ). One end of the joint was constrained using fixed support boundary conditions, restricting all degrees of freedom, while a prescribed displacement was applied incrementally at the opposite end to induce loading. Tensile loading conditions were simulated to capture the full debonding process. Incremental displacement control was adopted to ensure numerical stability and to accurately track damage initiation and propagation within the adhesive layer during loading.

2.2.4 Sensitivity Analysis

A comprehensive sensitivity analysis was conducted to evaluate the effects of key parameters on joint strength and debonding behavior. The investigated parameters include adhesive thick-

ness h_0 (1/10th h_0=0.12, 0.2, 0.5, 0.75 and 1.0), adhesive modulus, cohesive fracture toughness G_{IC}, fiber-to-matrix weight ratio, overlap length, and overlap width. To achieve optimal numerical accuracy, the adhesive layer mesh size was selected as one-tenth of the adhesive thickness. Each parameter was varied independently while keeping all other parameters constant, allowing the influence of individual factors on peel and shear stress distributions, failure modes, and maximum load capacity to be systematically evaluated.

2.2.5 Variational Method (Analytical Approach)

The variational method (VM) was employed as an analytical tool to validate the CZM Based FEM results and provide a comparative assessment of interfacial stress distributions. The method was based on solving the governing strain energy equations of the ABSSSJ using the principle of minimum potential energy ($0 \leq x \leq L$) [24]:

$$\begin{aligned} U = b\int_0^L \int_{-\frac{h_1}{2}}^{\frac{h_1}{2}} \left\{ \frac{1}{2}\left[\sigma_{xx}^{(1)}\epsilon_{xx}^{(1)} + \sigma_{yy}^{(1)}\epsilon_{yy}^{(1)}\right] + \frac{1+\nu_1}{E_1}\left[\tau_{xy_1}^{(1)}\right]^2 \right\} \mathrm{d}_x \mathrm{d}_y \\ + b\int_0^L \int_{-\frac{h_2}{2}}^{\frac{h_2}{2}} \left\{ \frac{1}{2}\left[\sigma_{xx}^{(2)}\epsilon_{xx}^{(2)} + \sigma_{yy}^{(2)}\epsilon_{yy}^{(2)}\right] + \frac{1+\nu_2}{E_2}\left[\tau_{xy_2}^{(2)}\right]^2 \right\} \mathrm{d}_x \mathrm{d}_{y_2} \\ + b\int_0^L \int_{-\frac{h_0}{2}}^{\frac{h_0}{2}} \left\{ \frac{1}{2}\left[\sigma_{xx}^{(0)}\epsilon_{xx}^{(0)} + \sigma_{yy}^{(0)}\epsilon_{yy}^{(0)}\right] + \frac{1+\nu_0}{E_0}\left[\tau_{xy_0}^{(0)}\right]^2 \right\} \mathrm{d}_x \mathrm{d}_{y_0} \end{aligned} \tag{3}$$

Under simplified boundary conditions such as uniform load, ideal adhesive properties, fixed support at one end, and displacement-controlled loading at the other-the VM was used to derive analytical expressions for peel and shear stresses within the adhesive layer (Eq. (1)). The analytical model assumes linear elastic material behavior and perfect bonding between adherends and adhesive. Unlike the CZM-based FEM, the variational method does not account for damage initiation or crack growth. Nevertheless, it provides closed-form stress solutions that serve as a benchmark for validating numerical predictions. The VM results were compared with CZM-based FEM outputs to assess the accuracy of the numerical model and to confirm the reliability of the predicted stress distributions.

2.3 Experimental Methods

2.3.1 Experimental Set-Up and Specimen Preparation

Test specimen for experimental validation of the adhesively bonded single-side strap joints (ABSSSJ) were fabricated using hybrid sisal-glass reinforced HDPE composite as the lower adherend and mild steel as the upper adherend. Both adherends were prepared with a uniform thicknesses of 2 mm. Three commercial structural adhesive in table 2 (Araldite 2015, Araldite 2020, and AV138) were employed to investigate the influence of adhesive type on joint performance. Adhesive bonding was carried out under controlled temperature and uniform pressure conditions to ensure consistent bond quality. Curing procedures followed the manufacturers' recommendations and were performed at 40°C for 2 h.

2.3.2 Hybrid Composite Fabrication

The hybrid sisal-glass reinforced HDPE composite was fabricated with the fiber-to-matrix weight ratio (30% fiber and 70% HDPE) (Table 1). Locally sourced sisal fibers were alkali-treated using a 5% NaOH solution for 4 h to remove surface impurities and enhance fiber–matrix adhesion but future work could explore optimization of this treatment. The treated fibers were cut to lengths of 25–30 mm and oven-dried at 80°C prior to composite fabrication. E-glass woven were introduced in the form of woven bidirectional mat with an areal density of 300 g/m^2 to enhance tensile stiffness and load-bearing capability. Hybrid stacking sequence of [S-G-G] and [G-S-G] were adopted to evaluate the influence of fiber arrangement on joint behavior. In these configurations, the outer glass layers increase bending stiffness and reduce peel stress, while the inner sisal layer contributed to weight reduction and improved energy absorption. The fibers oriented was maintained as [0/+45/90/-45/0] and [0/+45/90/-45/0] for all hybrid laminates.

2.3.3 Matrix Material

High-density polyethylene (HDPE) was selected as the thermoplastic matrix due to its low density, high impact resistance, ease of processing, and recyclability, making it suitable for lightweight automotive structures. The HDPE grade used in this study has a melt flow index of 6 g·10 min^{-1}, density of 0.96 g/cm^3, a tensile strength of 28 MPa, and melting temperature of

Table 1 Fiber to matrix ratio Hybrid Sisal-Glass Reinforced HDPE Composite

Ingredient	Composite Samples				
	$S_{25}G_5/H_{70}$	$S_{20}G_{10}/H_{70}$	$S_{15}G_{15}/H_{70}$	$S_{10}G_{20}/H_{70}$	S_5G_{25}/H_{70}
Sisal fiber(S)	25	20	15	10	5
Glass fiber(G)	5	10	15	20	25
HDPE(H)	70	70	70	70	70
Total	100	100	100	100	100

approximately 130°C. During composite fabrication, HDPE pellets were heated to 180–190°C to achieve complete melting and uniform wetting of both sisal and glass fibers, ensuring effective load transfer at the fiber–matrix interface.

2.3.4 Adhesive Layer and Surface Preparation

The adhesive layer was applied with controlled thicknesses of 0.2, 0.5, 0.75, and 1.0 mm to investigate the effect of bond-line thickness on peel and shear stress distributions (Table 2). Surface preparation of adherends was performed using silicon carbide sandpapers with grit sizes of 40, 60, 80, 100, and 120 to study the influence of surface roughness on adhesion strength. All bonded surfaces were cleaned prior to adhesive application to remove debris and contaminants.

Table 2 Physical, Mechanical Properties and parameters of ABSSSJ for Variational Method (VM), and Cohesive zone model (CZM) Based Finite element method (FEM)

Properties	Material-1		Material-2		Material-3		
	(upper) Adherend		Adhesive		(Lower) Adherend		
	Frame Mild steel	Araldite 2015	Araldite 2020	AV 138	Body Hybrid Composite		
Young Modulus (E)(Gpa)	200	1.85	2.57	3.5	16	70	1.35
Poisson Ratio (γ)	0.29	0.33	0.38	0.35	0.35	0.22	0.3
Tensile yield Strength (σy) (Gpa)	0.27	0.021	0.031	0.069	0.5	3.5	0.032
Shear modulus along plane (Gxy) (Gpa)	35	0.56	1.18	1.56	1.817	3.5	3.3
Density (δ) g/cm^3	7.85	1.1	1.2	1.25	1.5	2.5	0.96
Material Models	Linear-Elastic	Linear-Elastic	Linear-Elastic	Linear-Elastic	Non Linear-Inelastic-Bilinear		
Materials	Isotropic-Plane 182	Cohesive Element INTER 202			Orthotropic-Shell 181		
Length(mm)	25,half (12.5)	Bond length (half)=12.5, free edge length = 22.5			70 ,half(35)		
Thickness(mm)	steel 2mm	Adhesive 0.12, 0.2, 0.5, 0.75 and 1mm			Hybrid composite 2mm		
Debonding toughness	G_{IC} = 0.25, 0.5, 0.75, and 1.0kJ/m^2, G_{IIC} = 1.5 G_{IC}						
Adhesive to Adherends thickness ratio (ho/h2)	0.1, 0.25, 0.375, and 0.5						

2.3.5 Environmental Conditioning

To simulate service conditions relevant to automotive applications, bonded specimens were subjected to environmental conditioning prior to testing. Moisture exposure was introduced by immersing samples in water for durations of 2, 4, 6, 9, and 12 h. Additionally, specimens were exposed to elevated temperatures of 25, 30, 35, 40, and 45°C. These conditioning protocols enabled assessment of the combined effects of moisture and temperature on adhesive performance and joint durability.

2.3.6 Model Validation

Failure loads obtained from shear tests were compared with maximum loads predicted by numerical simulations. Sensitivity analyses were used to identify the most influential parameters affecting joint strength and failure behavior. In addition, statistical tools such as regression analysis and analysis of variance (ANOVA) were applied to quantify the relationships between adhesive properties, joint geometry, and mechanical performance.

2.4 Mechanical Testing

Mechanical testing was performed to evaluate the shear and tensile performance of the adhesively bonded single-side strap joints (ABSSSJ) and to validate the results obtained from

the cohesive zone model (CZM)–based finite element method (FEM) and the variational method (VM). All experiments were conducted using a universal testing machine (UTM, model WAW-600) with a maximum load capacity of 600 kN and a controllable crosshead speed ranging from 0.01 to 500 mm·min^{-1}.

Strain gauges were mounted in the vicinity near the adhesive interface to capture localized strain behavior during loading. The experimental program focused on determining the maximum shear stress, peel stress distribution, failure strain and dominant failure mode (adhesive, cohesive, or mixed-mode failure). Each test configuration was repeated three times to ensure repeatability and reliability of the results. Figure 1 illustrates the experimental setup and specimen configuration used for ABSSSJ testing. Displacement-controlled loading was applied until complete joint failure or full debonding occurred. Load–displacement data were continuously recorded to identify elastic response, damage initiation, and ultimate failure.

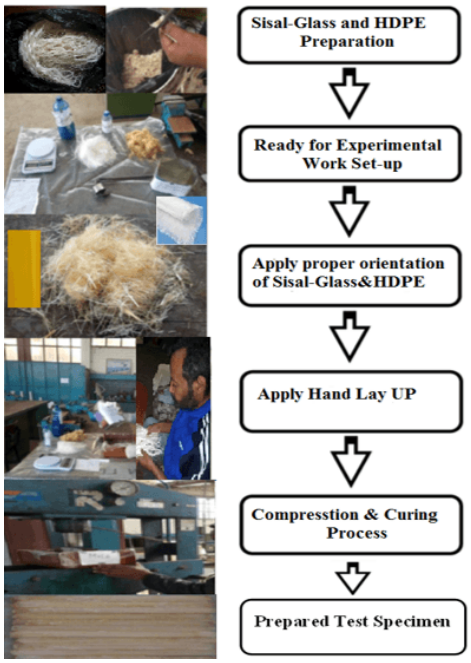

Figure 1 Illustrates the experimental set up and specimen configuration used for ABSSSJ testing

2.5 Sample Quantity and Statistical Analysis

For each test category, a total of 24 specimens were fabricated and tested. This included 18 specimens (6 configurations × 3 repetitions) for shear testing, three specimens for peel stress evaluation, and three specimens for FEM model validation. The average value obtained from three repeated tests specimens was used for final analysis. Standard deviation and error margins were calculated to quantify experimental scatter. Outliers were excluded only when deviations exceeded 10% from the mean value, in accordance with ASTM D1002 repeatability guidelines. This statistical treatment ensured data reliability and strengthened the correlation between experimental, numerical, and analytical results.

2.6 Data Analysis and Model Validation

Experimental results were systematically compared with predictions obtained from the variational method and CZM-based FEM simulations to assess the mechanical performance of the adhesive joints.

Peel and shear stress distributions derived from CZM Based FEM were evaluated against experimental measured responses, while variational method provided an analytical benchmark for model validation. Failure loads obtained from the shear tests were compared with the maximum loads predicted by numerical simulations. Sensitivity analyses were used to identify the most influential parameters affecting joint strength and failure behavior. In addition, Statistical tools, such as regression analysis and analysis of variance analysis (ANOVA) were applied to quantify the relationship between adhesive properties, joint geometry, and mechanical performance.

3 Results and Discussion

3.1 Computational Results

3.1.1 CZM based FEM Simulation Results

This section presents the computational results obtained from cohesive zone model (CZM)-based finite element modeling (FEM) simulations, supported by variational method (VM) calculations and experimental observations. The results were analyzed to evaluate the effects of key parameters on the mechanical strength, peel and shear stress distribution, and progressive debonding behavior of the adhesively bonded hybrid sisal–glass reinforced HDPE composite joints. Comparative discussions are provided to assess agreement among numerical, analytical, and experimental approaches, followed by interpretation of observed trends and failure mechanisms. CZM Based FEM was used to simulate the mechanical behavior of adhesively bonded single-side strap joint (ABSSSJ) and to analyze the stress distribution in the adhesive layer, and to capture the progressive debonding at the adhesive–adherend interface. Figure 2 illustrates the finite element model of the joint, including the upper steel adherend, lower hybrid composite adherend, and the intermediate adhesive layer developed in ANSYS.

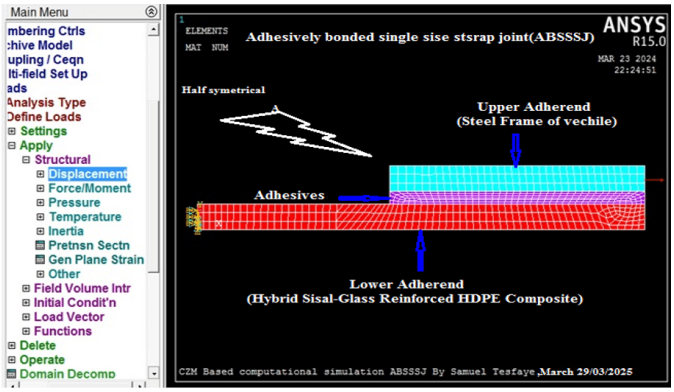

Figure 2 Illustrates the FEM Modeling of the joint including upper steel adherend, lower adherend and middle adhesive layer developed in ANSYS.

The geometry and mesh configuration are shown in Figure 3. The lower adherend was modeled as a hybrid sisal-glass reinforced HDPE composite using orthotropic shell elements (SHELL181) to account for anisotropic behavior arising from fiber orientation and stacking sequence.

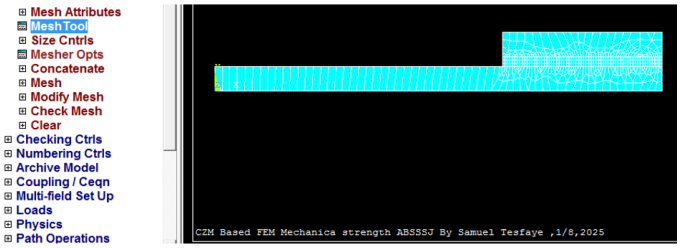

Figure 3 Geometry and Mesh Creation

The upper steel adherend was modeled using plane strain elements (PLANE182).The adhesive layer was discretized using cohesive interface elements (INTER202), enabling simulation of traction–separation behavior and debonding process.

Material properties for the hybrid composite, adhesive, and steel were assigned based on experimental characterization and literature data. The composite properties incorporated fiber-to-matrix weight ratio, fiber orientation, and stacking sequence, while adhesive properties included variations in elastic modulus, adhesive thickness, and cohesive fracture toughness. The steel adherend was assumed to be isotropic and characterized by Young's modulus and Poisson's ratio. The assigned material orientations and stacking sequences are illustrated in Figure 4.

Boundary conditions and loading configurations applied to the ABSSSJ are presented in

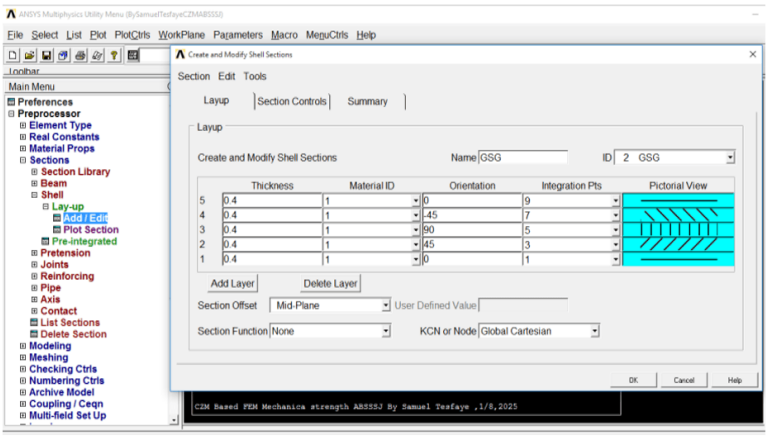

Figure 4 Illustrated material orientations and stacking sequence

Figure 5. One end of the joint was fully constrained, while displacement-controlled loading was applied at the opposite end to replicate experimental test conditions.

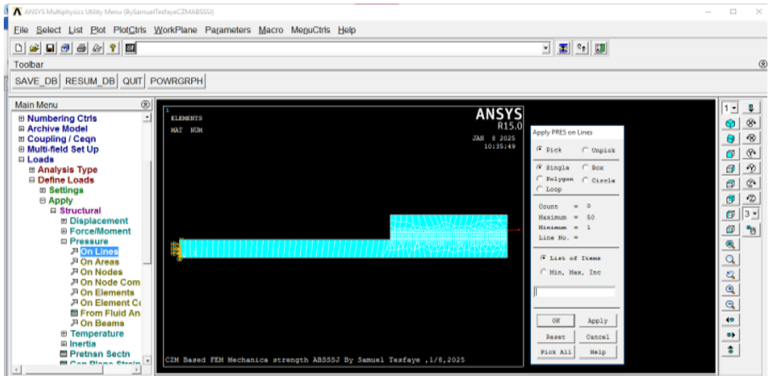

Figure 5 Boundary conditions and loading configurations applied to the ABSSSJ

Figure 6 provides a schematic overview of the applied constraints, convergence criteria, sensitivity analysis framework, and numerical stability considerations adopted in the CZM-based FEM simulations.

Discipline	Displacement Convergence		Force Convergence	
	Label	Label Description	Label	Label Description
Structural	U	Displacements	F	Forces
	ROT	Rotations	M	Moments

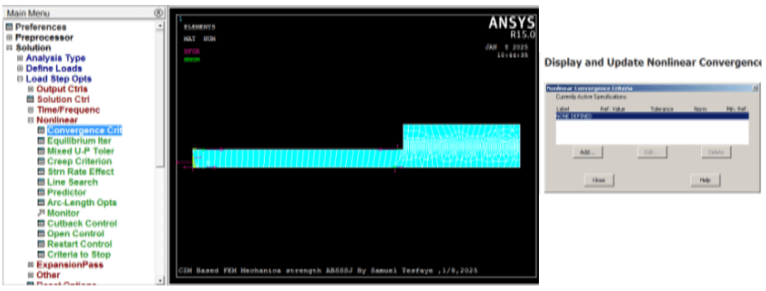

Figure 6 Schematic view applied constraints, convergence, sensitivity analysis frame work, numerical stability in the CZM-based FEM.

The von Mises stress distributions obtained from the simulations were shown in Figures 7 and 8.

High stress concentrations were observed overlap ends and adhesive–adherend interfaces,

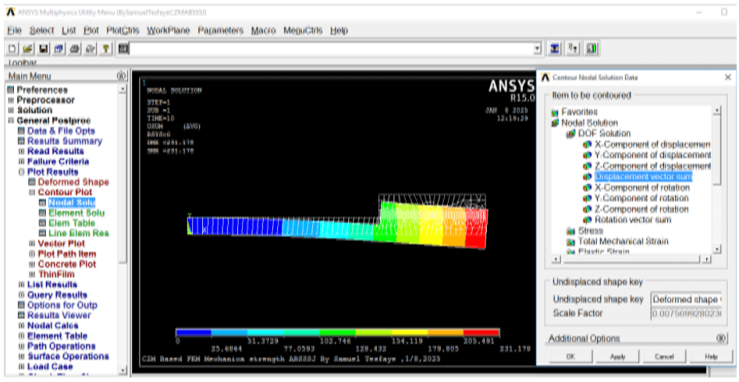

Figure 7 Solve simulation result von mises stress distribution Using CZM Based FEM of ABSSSJ

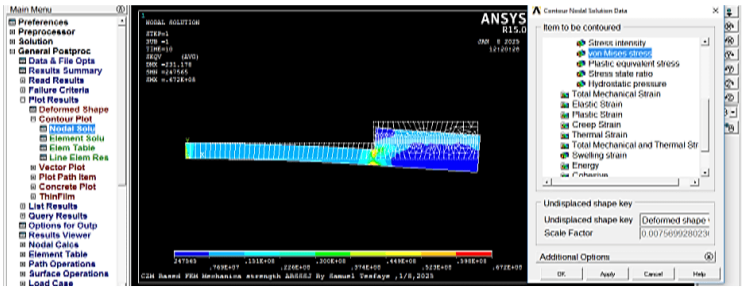

Figure 8 Solve simulation result von mises stress distribution using CZM Based FEM of ABSSSJ

indicating potential locations for damage initiation and debonding under increasing load. Figure 9 presents the corresponding peel and shear stress distributions within the adhesive layer.

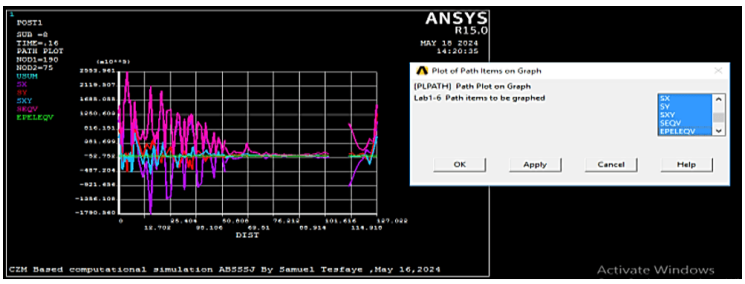

Figure 9 Illustrate peel and shear stress distribution within the adhesive layer

3.1.2 Stress Distribution in the Adhesive Layer

The CZM based FEM simulations provide detailed insight into the peel and shear stresses distribution within the adhesive layer of ABSSSJ under applied loading conditions. The results demonstrate significant stress gradients across the overlap length and adhesive thickness highlighting critical regions susceptible to failure initiation. Peel stress were found to be maximum at the edges of the adhesive layer, particularly near the ends of the overlap region. The magnitude of peel stress gradually decreases towards the middle of the bondline. This behavior was consistent with classical adhesive joint mechanics, where bending-induced tensile stresses dominate near the overlap edges, promoting crack initiation at these locations. Shear stresses were primarily concentrated near the overlap ends but exhibited a more uniform distribution across the central region of the adhesive layer. Compared with peel stresses, shear stresses showed lower sensitivity to adhesive thickness but were influenced by adherend stiffness and overlap geometry. The dominance of shear stress in the mid-bond region confirms the load-transfer role of the adhesive layer in ABSSSJ configurations. Overall, the stress distribution patterns predicted by the CZM-based FEM align well with theoretical expectations and experimental observations. The combined presence of high peel stress at the overlap edges

and elevated shear stress near the bondline ends explains the observed debonding behavior and failure modes in hybrid sisal–glass reinforced HDPE composite joints.

3.2 Variational Method (VM) Results of ABSSSJ

The variational method (VM) was employed as an analytical approach to validate the cohesive zone model (CZM)–based finite element method (FEM) results and to provide a comparative assessment against experimental observations for adhesively bonded single-side strap joints (ABSSSJ). The VM enables closed-form estimation of peel and shear stresses in the adhesive layer and adherends based on strain energy minimization, thereby serving as a benchmark for evaluating numerical predictions.

3.2.1 Planar Stress Results from the Variational Methods

Tables 3, 4, and 5 summarizes the planar stress results obtained using the variational method for the upper adherend (steel), adhesive layer, and lower adherend (hybrid sisal–glass reinforced HDPE composite). Static equilibrium conditions in terms of axial force ($\sum F_x$), transverse force ($\sum F_y$), and bending moment ($\sum$ M) were satisfied for the upper adherend, adhesive layer, and lower adherend under applied loading. For the adhesive layer, the axial force and bending moments increased with adhesive thickness (h_0 = 0.2–1.0 mm), indicating a strong dependence of bending-induced peel stresses on bond-line thickness. In contrast, the analytical solution predicted negligible shear stress and transverse peel stress within the adhesive layer under the assumed ideal bonding and linear elastic conditions. This limitation highlights the simplified nature of the variational approach, which does not account for damage initiation or interfacial nonlinearity. The upper steel adherend exhibited increasing bending moments with increasing adhesive thickness, while axial forces remained relatively constant. For the lower hybrid composite adherend, peel (normal) stresses were predicted to be uniform across the overlap length and independent of adhesive thickness, reflecting the assumptions of perfect bonding and continuous load transfer inherent in the analytical model.

3.2.2 Peel Stress Distribution in the Middle of Adhesive Layers

Figure 10 presents the peel stress distribution in the middle of the adhesive layer along the normalized overlap length (x/l) as predicted by the variational method, CZM-based FEM, and experimental measurements. The VM results indicate that peel stress reaches its maximum magnitude at the overlap ends (x/l = $\pm$1.0) and decreases progressively toward the mid-span (x/l = 0), resulting in a symmetric stress distribution about the joint centerline.

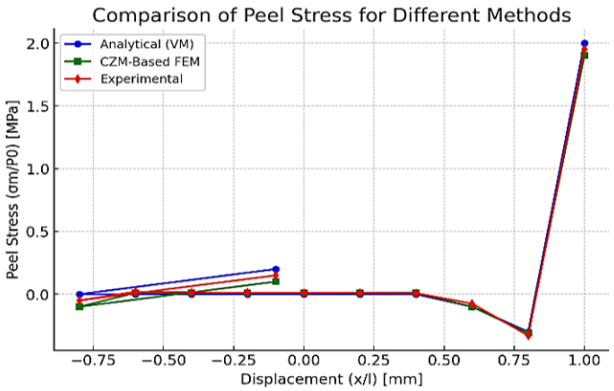

Figure 10 Peel Stress distribution in the middle of adhesive layers in the ABSSSJs

Compressive peel stresses were observed in the central region of the adhesive layer, while tensile peel stresses dominated near the overlap edges. The high stress concentration at the bond-line edges confirms that these regions are the most susceptible to crack initiation and subsequent debonding.

3.2.3 Comparison with CZM-Based FEM and Experimental Results

A comparative analysis of peel stress distributions reveals notable differences among the three approaches. The variational method slightly overestimated peel stresses at low displacement levels and underestimated stresses in the intermediate overlap region. In contrast, the CZM-based FEM predictions closely followed the experimental results across the entire overlap length, capturing both localized stress variations and non-zero intermediate stresses that the analytical

Table 3 Summery results of Static equilibrium in Adherends (upper and lower) and adhesive layers of (ABSSSJ) of Analytical using Variational method (VM)

Properties		Material -1	Material -2			Material-3		
		(Upper) Adherened	Adhesive			(Lower) Adherend		
		Frame Mild steel	Araldite 2015	Araldite 2020	Araldite AV 138	Body Hybrid Composite		
						Sisal	E-Glass	HDPE
Static equilibrium at upper Adherend	$\sum F_x$	-175×10^6 N	-	-	-	-	-	
	$\sum F_y$	-1.35×10^9 N	-	-	-	-	-	
	$\sum M$	-1.52×10^9 N · m	-	-	-	-	-	
Static equilibrium at lower Adherend	$\sum F_x$	-	-	-	-	9×10^9 N	1.8×10^{10} N	2×10^7 N
	$\sum F_y$	-	-	-	-	2×10^9 N	1.8×10^{10} N	2×10^7 N
	$\sum M$	-	-	-	-	-1×10^9 N · m	2×10^7 N · m	-2×10^7 N · m
Static equilibrium of middle Adhesive	$\sum F_x$	-	1.66×10^{11} N	1.575×10^{11} N	1.585×10^{11} N	-	-	
	$\sum F_y$	-	-9.9×10^8 N	-1.6×10^{10} N	1.19×10^9 N	-	-	
	$\sum M\ (h_0 = 0.2)$	-	-1.84×10^{10} N · m	-1.9×10^{10} N · m	-19.2×10^{10} N · m	-	-	
	$\sum M\ (h_0 = 0.5)$	-	-4.6×10^{10} N · m	-4.8×10^{10} N · m	-47.8×10^{10} N · m	-	-	
	$\sum M\ (h_0 = 0.75)$	-	-6.88×10^{10} N · m	-7.2×10^{10} N · m	-71.8×10^{10} N · m	-	-	
	$\sum M\ (h_0 = 1.0)$	-	-9.2×10^{10} N · m	9.6×10^{10} N · m	-95.7×10^{10} N · m	-	-	

Table 4 Summery results of Axial, shear and bending moments in Adherends (upper and lower) and ad-hesive layers of (ABSSSJ) of Analytical using Variational method (VM)

Properties		Material -1	Material -2			Material-3		
		(Upper) Adherened	Adhesive			(Lower) Adherend		
		Frame Mild steel	Araldite 2015	Araldite 2020	Araldite AV 138	Body Hybrid Composite		
						Sisal	E-Glass	HDPE
Upper Adherend(frame)	Axial force (S1)	2.1×10^8 N	-	-	-	-	-	-
	Shear force (Q1)	0	-	-	-	-	-	-
	Bending moments ($\sum M$) (h_0 = 0.2)	4.6×10^8 N · m	-	-	-	-	-	-
	Bending moments ($\sum M$) (h_0 =0.5)	5.25×10^9 N · m	-	-	-	-	-	-
	Bending moments ($\sum M$) (h_0 = 0.75)	5.8×10^9 N · m	-	-	-	-	-	-
	Bending moments ($\sum M$) (h_0 = 1.0)	6.3×10^8 N · m	-	-	-	-	-	-
Lower Adherend (Body)	Axial force (S2)	-	-	-	-	-	2.1×10^9 N	-
	Shear force (Q2)	-	-	-	-	-	0	-
	Bending moments ($\sum M2$)	-	-	-	-	-	0	-
Adhesive Adherend (middle)	Axial force (S0)	-	-	-	-	-	0	-
	Shear force (Q0)	-	-	-	-	-	0	-
	Bending moments ($\sum M0$)	-	-	-	-	-	0	-

Table 5 Summery results of interfacial (shear and peel) stress in Adherends (upper and lower) and adhesive layers of (ABSSSJ) of Analytical using Variational method (VM)

Properties		Material -1	Material -2			Material-3		
		(Upper) Adherened	Adhesive			(Lower) Adherend		
		Frame Mild steel	Araldite 2015	Araldite 2020	Araldite AV 138	Body Hybrid Composite		
						Sisal	E-Glass	HDPE
Upper Adherend planar stress (τ_1&σ_1)	Interfacial Shear stress $\tau_{yx}^{(1)}$	18.4×10^6 Pa	-	-	-	-	-	-
	Peel stress $\sigma_{xx}^{(1)}$	84.48×10^6 Pa	-	-	-	-	-	-
	Peel (tran.) stress $\sigma_{yy}^{(1)}$	0	-	-	-	-	-	-
Lower Adherend planar stress (τ_1&σ_1)	Interfacial Shear stress $\tau_{yx}^{(2)} = 0$	-	-	-	-	-	0	-
	Peel (normal) stress $\sigma_{xx}^{(2)}$	-	-	-	-	-	2.18×10^8 Pa	-
	Peel (tran.) stress $\sigma_{yy}^{(2)}$	-	-	-	-	-	0	-

model failed to predict. Experimental measurements exhibited slightly positive peel stresses in the mid-region, whereas the variational method predicted near-zero values due to its simplifying assumptions. Negative peel stress trends were observed in both experimental and numerical results at certain locations, indicating stress reversals that may influence fatigue behavior. Error analysis further confirms the superior predictive capability of the CZM-based FEM. The mean absolute error (MAE) between analytical and experimental results was 0.0255 MPa, compared to 0.0196 MPa for CZM-based FEM. Similarly, the root mean square error (RMSE) values were 0.0302 MPa and 0.0281 MPa, respectively. The mean percentage error (MPE) highlights significant underestimation by the variational method (-58.17%), whereas CZM-based FEM showed close agreement with experiments (1.67%), therefore the VM should be considered a preliminary design tool, while CZM-based FEM recommended for accurate and structural optimization.

Sensitivity of VM Results to Adhesive Thickness: An analytical sensitivity assessment was added to evaluate the influence of adhesive thickness (t_α) on VM predictions: VM predicts that: Shear and peel stresses are inversely proportional to adhesive thickness (*i.e.*, $\tau, \sigma \propto 1/t_\alpha$). As adhesive thickness increases: Predicted stresses decrease due to reduced stiffness of the adhesive layer , and Stress gradients become smoother, further suppressing localized peaks. However, VM does not capture: Nonlinear stress redistribution at higher thicknesses, and Transition from adhesive to cohesive failure modes. This explains why VM: Shows monotonic trends, and Fails to reproduce the experimentally observed optimal thickness behavior.

3.2.4 Implications for Mechanical Strength and Joint Design

The peel stress analysis demonstrates that the overlap edge ($x/l \approx 1.0$) is the most critical location for failure initiation in ABSSSJ, with peak experimental peel stresses of approximately 1.95 MPa. The ability of CZM-based FEM to accurately capture this peak stress and its distribution confirms its suitability for predicting joint strength and failure behavior. The analytical variational method, while useful for trend analysis and preliminary design, is limited in its ability to capture localized stress concentrations and progressive damage. Design improvements such

as adhesive edge tapering, optimization of adhesive thickness, and increased cohesive fracture toughness are recommended to reduce stress concentrations and enhance joint performance. Overall, the variational method provides valuable analytical insight, but the CZM-based FEM approach offers a more realistic and reliable prediction of peel stress distribution and mechanical strength for adhesively bonded hybrid sisal–glass reinforced HDPE composite joints intended for automobile side body panel applications.

3.3 Shear Stress Distribution in the Middle of Adhesive Layers

This section presents and discusses the shear stress distribution in the middle of the adhesive layer of adhesively bonded single-side strap joints (ABSSSJ), based on analytical variational method (VM), cohesive zone model (CZM)–based finite element method (FEM), and experimental results.

3.3.1 Shear Stress Distribution Characteristics

The shear stress distribution along the normalized overlap length (x/l) exhibited a predominantly parabolic profile, with maximum shear stress occurring near the central region of the adhesive layer (x/l $\approx$ 0) and minimum values observed toward the overlap edges (x/l = $\pm$1.0), as shown in Figure 11. This behavior is consistent with classical load-transfer mechanisms in adhesively bonded joints, where shear stress dominates in the mid-overlap region, while peel stress governs near the bond-line edges. Unlike peel stress, shear stress did not exhibit sign reversal across most of the overlap length under moderate loading conditions. The central region of the adhesive layer therefore represents a critical zone under high shear loading, particularly when adhesive stiffness or overlap length is not optimized.

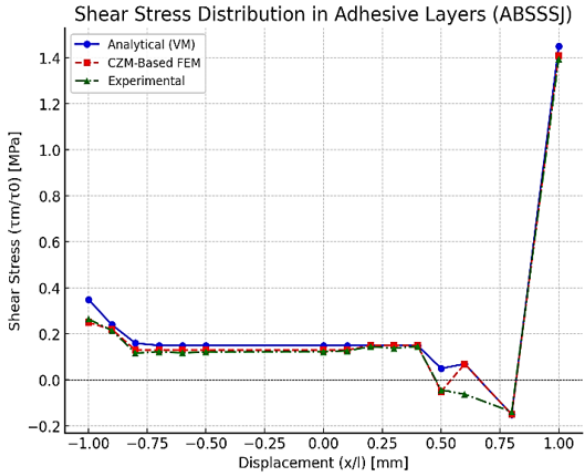

Figure 11 Shear Stress distribution in the middle of adhesive layers in the ABSSSJs

3.3.2 Comparison of Analytical, Numerical, and Experimental Results

A detailed comparison among VM, CZM-based FEM, and experimental results reveals distinct differences in predictive capability across the overlap length. Maximum shear stress region (x/l $\approx$ -1.0 to -0.8).The analytical variational method predicted the highest shear stress at x/l = -1.0 ($\approx$ 0.35 MPa), while CZM-based FEM predicted lower values ($\approx$ 0.25 MPa). Experimental measurements closely followed the CZM-based FEM predictions ($\approx$ 0.265 MPa), indicating that FEM provides a more realistic representation of actual joint behavior. The analytical method consistently overestimated shear stress in this region. Quasi-uniform shear stress region (x/l $\approx$ -0.8 to 0.4).Between x/l = -0.8 and 0.4, shear stress remained nearly constant for CZM-based FEM and experimental results, with values ranging from approximately 0.13 to 0.15 MPa. The analytical method predicted slightly higher stresses ($\sim$0.15 MPa), indicating a small but consistent deviation. This region highlights the superior accuracy of CZM-based FEM in capturing realistic stress redistribution. Negative shear stress region (x/l $\approx$ 0.5 to 0.8). At x/l $\approx$ 0.5, experimental shear stresses transitioned into negative values ($\approx$ -0.043 MPa), with more pronounced negative stresses observed at x/l $\approx$ 0.8 ($\approx$ -0.138 MPa). CZM-based FEM accurately captured this stress reversal, whereas the analytical method exhibited delayed transition, demonstrating its limitation in modeling shear stress sign changes. Peak shear stress at extreme displacement (x/l $\approx$ 1.0).At x/l = 1.0, all three approaches predicted a significant

shear stress peak of approximately 1.4 MPa. The analytical method slightly overestimated the peak value (∼1.45 MPa), while CZM-based FEM and experimental results showed closer agreement, confirming strong adhesive load transfer at large displacements.

3.3.3 Model Accuracy and Interpretation

Overall, CZM-based FEM demonstrated the closest agreement with experimental data across all regions of the overlap length, accurately capturing peak stresses, stress plateaus, and stress reversals. The analytical variational method provided reasonable trend predictions but consistently overestimated stress magnitudes and struggled to represent negative shear stress regions due to its simplifying assumptions. These findings confirm that CZM-based FEM was the most reliable approach for predicting shear stress distribution in adhesively bonded hybrid sisal–glass reinforced HDPE composite joints.

3.3.4 Design Implications for ABSSSJ

The results indicate that both the central region and overlap edges of the adhesive layer were critical under shear loading, depending on displacement level and loading condition. Optimizing adhesive modulus, overlap length, and adhesive thickness can significantly reduce peak shear stress and improve load distribution. Additionally, accurate prediction of stress reversals was essential for assessing fatigue performance and long-term durability. The strong agreement between CZM-based FEM and experimental results demonstrates the suitability of the numerical framework for joint design and optimization in automobile side body panel applications.

3.3.5 Peeling Stress Distribution b/n Upper adherened and Adhesive Layers in the ABSSSJs

This section presents the peeling stress distribution between the upper steel adherend and the adhesive layer in the adhesively bonded single-side strap joint (ABSSSJ). The results obtained using the analytical variational method (VM), cohesive zone model (CZM)–based finite element method (FEM), and experimental measurements were compared and discussed to evaluate stress transfer behavior and failure initiation mechanisms.

3.3.6 Peeling Stress Distribution Trend

Figure 12 illustrates the normalized peeling stress distribution (σ_{3y}/P_0) along the overlap length (x/l) between the upper adherend and the adhesive layer. The results show that the peeling stress attains its maximum magnitude at the overlap edges (x/l=±1.0)(x/l = ± 1.0)(x/l=±1.0) and gradually decreases toward the center of the joint (x/l=0). This trend is characteristic of adhesively bonded joints, where stress concentrations develop at the free edges of the adhesive layer due to bending and load eccentricity.

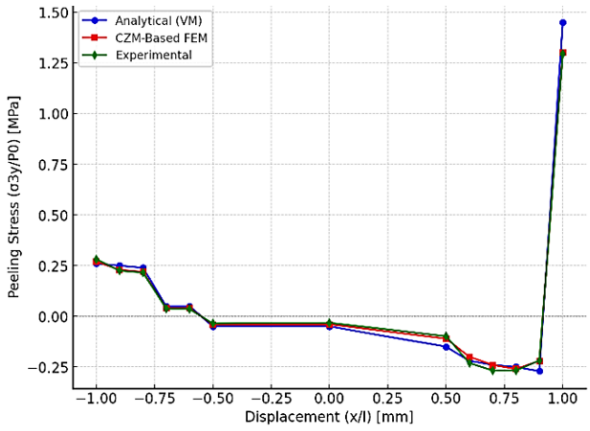

Figure 12 Peeling Stress distribution b/n upper adherened and adhesive layers in the ABSSSJs

Compared with the peel stress distribution in the middle of the adhesive layer, the peak stress values at the upper adherend–adhesive interface were slightly lower, indicating partial stress redistribution through the adhesive thickness. However, a sharper stress gradient was observed near the upper adherend, highlighting the increased sensitivity of this interface to adhesive thickness variation and surface preparation conditions. Negative peel stress values were observed in the central region of the overlap, indicating compressive stresses that may contribute to reduced likelihood of crack initiation at the joint center.

3.3.7 Comparison of VM, CZM-Based FEM, and Experimental Results

The analytical variational method predicted a peak peeling stress of approximately 1.45 MPa at x/l=1.0x/l = 1.0x/l=1.0, which is slightly higher than the corresponding values obtained from CZM-based FEM (1.34 MPa) and experimental measurements (1.32 MPa). Across the overlap length, the CZM-based FEM results closely followed the experimental data, demonstrating the capability of the numerical model to accurately capture localized stress variations and interfacial behavior. The analytical method consistently overestimated peeling stresses due to simplifying assumptions, including linear elastic material behavior and idealized interfacial bonding. In contrast, CZM-based FEM accounted for traction–separation behavior and progressive debonding, resulting in improved agreement with experimental observations.

3.3.8 Model Accuracy and Failure Implications

The deviation between CZM-based FEM and experimental results remained within approximately 5%, indicating good predictive accuracy. Minor discrepancies can be attributed to experimental uncertainties such as adhesive thickness variation, surface roughness, manufacturing defects, and test alignment. The pronounced stress concentration at the overlap edges suggests that debonding was most likely to initiate at these locations. Conversely, compressive peel stresses in the mid-overlap region reduce the probability of failure initiation at the joint center.

3.3.9 Design Implications

The results emphasize the importance of surface treatment of the upper adherend in minimizing peak peeling stresses. Improved surface preparation, appropriate sand grade selection, and optimized adhesive thickness can significantly reduce stress concentration. Additionally, gradual tapering of the upper adherend edges may further alleviate peel stress peaks and enhance joint durability. Overall, the findings confirm that CZM-based FEM provides a reliable and accurate tool for predicting peeling stress distribution, offering valuable insights for the design and optimization of adhesively bonded hybrid sisal–glass reinforced HDPE composite joints intended for automobile side body panel applications.

3.4 Peel Stress Distribution between the Lower Adherend and Adhesive Layers in ABSSSJs

Figure 13 illustrates the peel stress distribution at the interface between the lower adherend and the adhesive layer in ABSSSJs, obtained using the analytical variational method (VM), cohesive zone model (CZM)-based finite element method (FEM), and experimental measurements.

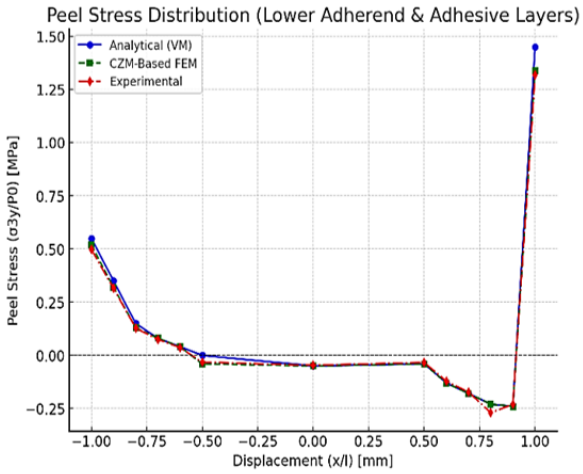

Figure 13 Peel stress distribution between the lower adherened and adhesive layers in ABSSSJs

Peel Stress Distribution Characteristics: The peel stress (σ_{3y}/P_0) exhibits a symmetric distribution along the normalized overlap length (x/l). The maximum peel stresses occur at the edges of the bonded joint (x/l = $\pm$1.0), while the stress magnitude reduces toward the center of the overlap, approaching near-zero values at x/l = 0. Negative peel stress values observed in the central region indicate the presence of local compressive stresses at the adhesive–

adherend interface. This stress distribution pattern is characteristic of adhesively bonded single-strap joints, where stress concentrations at the overlap edges significantly influence failure initiation. Comparison of Analytical, Numerical, and Experimental Results: The analytical VM predicts a peak peel stress of 1.45 MPa at x/l = $\pm$1.0, which was slightly higher than the corresponding values obtained from the CZM-based FEM (1.34 MPa) and experimental measurements (1.32 MPa). Across the entire overlap length, the CZM-based FEM results closely follow the experimental data, demonstrating strong agreement between numerical simulation and physical testing. The minor deviations observed between the analytical and experimental results can be attributed to the simplifying assumptions inherent in the variational method, which does not fully account for adhesive nonlinearity, localized plastic deformation, or damage evolution at the interface.

Failure Initiation and Stress Interaction: The concentration of peel stress at the overlap edges indicates that these regions were the most critical zones for damage initiation and debonding. In contrast, the central region of the adhesive layer experiences comparatively lower peel stresses and dominant shear stress contributions. Under extreme loading conditions, this stress interaction suggests that peel-driven failure is more likely to initiate at the edges, whereas shear-driven failure may occur near the mid-overlap region. Validation and Engineering Implications:- The close agreement between CZM-based FEM and experimental results, with deviations within approximately 5%, confirms the reliability of the cohesive zone modeling approach for predicting peel stress behavior in hybrid sisal–glass fiber reinforced HDPE composite joints. The small discrepancies may be influenced by experimental uncertainties such as adhesive thickness variation, manufacturing imperfections, and testing conditions. The observed stress concentration at the overlap edges highlights the need for design optimization strategies, including modification of overlap length, adhesive thickness, surface treatment, and localized reinforcement, to reduce peak peel stresses and enhance joint durability. Furthermore, the compressive peel stress observed in the central region may contribute to improved resistance against premature failure. Future Work: Further studies could include sensitivity analyses on adhesive material properties such as elastic modulus and fracture toughness, as well as investigations into environmental effects such as temperature and moisture exposure. Incorporating advanced adhesive material models, including nonlinear and viscoelastic behavior, may further improve the predictive capability of CZM-based FEM simulations and provide deeper insights into failure mechanisms.

3.5 Experimental Results

Experimental investigations were conducted to evaluate the mechanical performance and failure behavior of adhesively bonded single-strap joints (ABSSSJs) fabricated using hybrid sisal–glass fiber reinforced HDPE composites. The experimental results were used to validate the cohesive zone model (CZM)-based finite element method (FEM) predictions and to assess the influence of adhesive and reinforcement parameters under shear and tensile loading conditions.

3.5.1 Shear and Tensile Testing

Shear and tensile tests were performed using a universal testing machine (UTM) to determine the load-carrying capacity and deformation characteristics of the bonded joints and composite adherends. Shear Test Results: Lap shear tests were conducted in accordance with ASTM D5868-01 (2008) to evaluate the shear strength of the ABSSSJ specimens. The results indicated a well-defined failure point in all tested specimens. The maximum shear strength was strongly influenced by adhesive thickness, adhesive elastic modulus, and fiber-to-matrix weight ratio. Specimens with thinner adhesive layers exhibited higher shear strength due to reduced stress concentrations at the adhesive–adherend interface. Increased adhesive thickness resulted in improved load distribution but led to localized shear stress amplification near the overlap entrance. Figure 14 presents the experimental setup and post-test condition of the shear-tested specimens, including the UTM configuration, specimen geometry, and observed failure features.

Tensile Test Results of Hybrid Composite Adherends: Tensile tests were conducted on the hybrid sisal–glass composite adherends to evaluate the influence of fiber stacking sequence on tensile performance. The results demonstrated that tensile strength was significantly affected by fiber orientation and layer configuration due to the effect of stacking sequence had now been explicitly clarified using experimental findings: The G–S–G stacking sequence achieved the highest tensile strength (62.3 MPa), indicating superior load transfer. Mechanistically: Glass fiber outer layers (G–S–G): Provide higher surface stiffness, Reduce deformation mismatch with steel adherend, Lower interfacial shear and peel stress gradients, Sisal-rich outer layers: Lower stiffness, Increase strain incompatibility, Promote stress localization and earlier debonding. Hybridization improves: Stress redistribution, Crack bridging and arrest mechanisms. Thus,

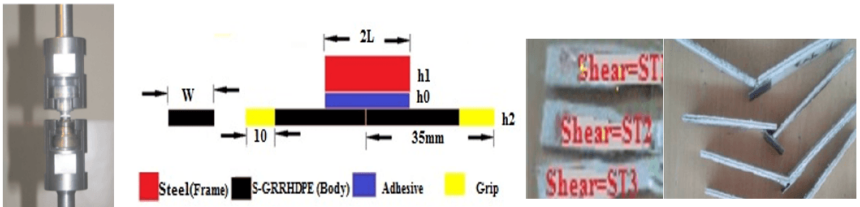

(a) (b) (c)

Figure 14 (a) Universal testing machine (UTM) used for shear testing, (b) specimen dimensions, and (c) ABSSSJ specimen after shear testing.

stacking sequence directly governs interfacial stress distribution, crack initiation sites, and overall joint durability, which has been clarified in the revised manuscript. Figure 15 illustrates the tensile test setup and post-failure condition of the lower adherend, while Figure 16 compares the tensile responses of different stacking sequences.

(a) (b)

Figure 15 (a) Tensile testing using UTM and (b) hybrid composite specimen after tensile testing (lower adherend)

Figure 16 Tensile test results for different stacking sequence (a) Glass-Sisal-Glass, (b) Sisal-Glass-Glass.

3.5.2 Failure Modes

The experimentally observed failure modes were consistent with the trends predicted by the CZM-based FEM simulations, confirming the accuracy of the numerical modeling approach. Adhesive debonding was the predominant failure mode observed during shear testing. Debonding primarily initiated at the edges of the adhesive layer, where peak peel stresses were concentrated. This failure mode was dominant in specimens with thinner adhesive layers and lower adhesive toughness. Figure 17 shows representative failure surfaces after shear testing, clearly indicating adhesive debonding at the adhesive–adherend interface.

Figure 17 Failure modes after shear testing of results ABSSSJ specimens adhesive debonding

The main failure modes were: Adhesive Debonding: In most cases, the adhesive layer failed due to debonding, particularly at the edges of the adhesive layer where the peel stress was highest. This was the most common failure mode observed in the shear tests due to material

mismatch between adherends, peel stress localization, surface and interfacial limitations. The effect of adhesive thickness on debonding behavior is illustrated in Figure 18, where increased adhesive thickness resulted in delayed crack initiation but altered the stress transfer mechanism.

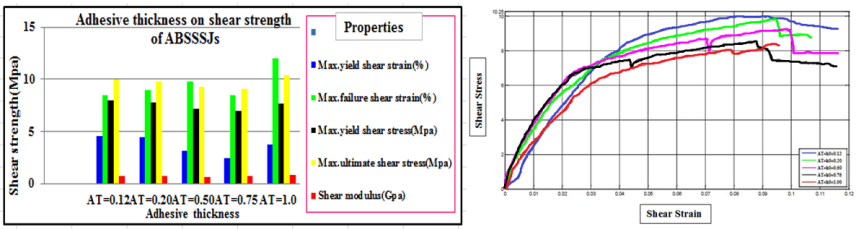

Figure 18 Effect of adhesive thickness on adhesive debonding failure modes in ABSSSJ

Cohesive failure within the adhesive layer was observed in a limited number of specimens, particularly those with higher adhesive modulus. Although less frequent than adhesive debonding, cohesive failure indicates improved interfacial bonding and enhanced energy dissipation capability of the adhesive layer. The influence of debonding toughness on force–displacement behavior is presented in Figure 19, demonstrating increased load-bearing capacity and delayed failure with higher adhesive toughness.

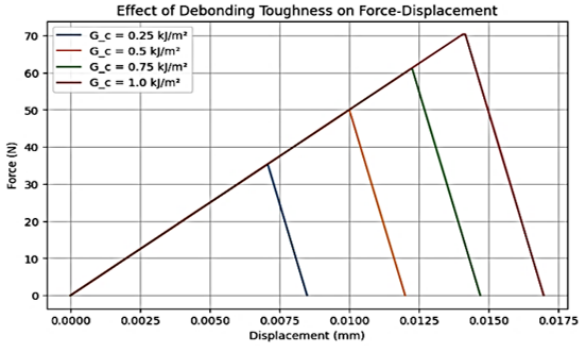

Figure 19 Effect of debonding tough on force-displacement response of ABSSSJ

3.5.3 Correlation between Experimental and Numerical Results

The CZM-based FEM simulations revealed a highly non-uniform stress distribution along the adhesive interface. Peak peel stresses in the range of 2.85–3.12 MPa were observed near the free edges, while peak shear stresses of 9.44–10.21 MPa occurred at the overlap entrance.Hybrid sisal–glass reinforcement reduced peak peel stress by approximately 14.7% compared to pure sisal–HDPE joints and enhanced shear load transfer by 12.3%, owing to improved stiffness distribution across the adherend layers. These improvements contributed to delayed crack initiation and enhanced joint durability. Experimental shear testing yielded an average ultimate shear load of 4.68 kN, while the FEM predicted 4.52 kN, resulting in a deviation of 3.4%, which is within acceptable engineering limits. Additionally, the peel failure initiation locations predicted by FEM closely matched the experimental fracture surfaces, with a positional deviation of less than 6%, further validating the CZM model.

3.5.4 Influence of Adhesive and Hybrid Reinforcement Parameters

Increasing adhesive thickness from 0.2 mm to 0.75 mm reduced peak peel stress by 21.9%, although it led to a 9.6% increase in shear stress. An adhesive modulus in the range of 1.85–2.5 GPa provided an optimal balance between stiffness and flexibility. Hybrid sisal–glass reinforcement improved the load-carrying capacity of ABSSSJs by approximately 18–25% compared to single-fiber systems. The hybridization mechanism effectively combined the high stiffness of glass fibers with the energy absorption capability of sisal fibers, resulting in a stable peel–shear stress distribution suitable for automotive side panel bonding applications.

4 Conclusion

This study presented a comprehensive computational and experimental investigation of peel and shear stress distributions in adhesively bonded single-side strap joints (ABSSSJ) composed

of steel and hybrid sisal–glass reinforced HDPE composite, specifically targeted for automobile side body panel applications. The conclusions directly address the objectives established in the Introduction and are supported by results discussed in Sections 3.1–3.6.

Cohesive zone model (CZM)–based finite element method (FEM) simulations demonstrated excellent capability in predicting joint behavior, including stress distribution, damage initiation, crack propagation, and progressive debonding. The numerical results showed strong agreement with experimental observations, confirming the reliability of the developed FEM framework for analyzing adhesively bonded hybrid composite joints. Deviations between FEM predictions and experimental results were limited to approximately 3.4% for ultimate shear load and less than 6% for crack initiation location, validating the accuracy of the proposed model.

Both peel and shear stress distributions were found to be highly non-uniform along the overlap length. Peak peel stresses were concentrated near the overlap edges, while shear stresses dominated the central region of the adhesive layer. The CZM-based FEM successfully captured negative peel stress regions in the mid-overlap zone and stress reversals at higher displacements, phenomena that were not adequately represented by the analytical variational method. This highlights the limitations of simplified analytical models for predicting localized interfacial behavior.

Parametric investigations revealed that adhesive thickness, adhesive modulus, fiber-to-matrix weight ratio, surface sand grade, moisture exposure, and temperature significantly influence joint strength and debonding behavior. An adhesive thickness of approximately 0.75 mm and an adhesive modulus in the range of 1.85–2.5 GPa were found to minimize peel stress concentrations without compromising shear load transfer. Hybrid sisal–glass reinforcement reduced peel stress concentration by approximately 14–15% and improved joint load-carrying capacity by 18–25%, demonstrating its effectiveness for lightweight automotive structures.

Overall, the combined use of CZM-based FEM, experimental validation, and analytical comparison provides a robust and application-specific understanding of peel and shear stress behavior in steel-to-hybrid sisal–glass reinforced HDPE adhesive joints. The findings fill a critical knowledge gap in the design of natural–synthetic hybrid composite joints and confirm their suitability for automobile side body panel applications.

Author Contributions

Samuel Tesfaye Molla: Conceptualization, study design, original draft preparation and final draft revision; Assefa Asmare Tsegaw: Literature review and data analysis; Teshome Mulatie Bogale: Writing—original draft preparation; Addisu Negash Ali and Asmamaw Tegegne Abebe: Writing—review and editing.

Acknowledgements

The authors would like to thank Bahirdar Institute of Technology, BIT for access to research facilities and digital databases.

Conflicts of Interest

The authors declare that they have no conflicts of interest.

References

[1] Adams RD, Peppiatt NA. Stress analysis of adhesive-bonded lap joints. Journal of Strain Analysis. 1974, 9(3): 185-196. https://doi.org/10.1243/03093247v093185

[2] Karthikeyan N, Naveen J. Progress in adhesive-bonded composite joints: A comprehensive review. Journal of Reinforced Plastics and Composites. 2024, 44(19-20): 1844-1890. https://doi.org/10.1177/07316844241248236

[3] Raj MKA, Kumar PM, Palanisamy P, et al. Study on the mechanical characteristics of a natural Fiber-based hybrid polymer composite. Scientific Reports. 2025, 15(1). https://doi.org/10.1038/s41598-025-29459-4

[4] Kaleel I, Carrera E, Petrolo M. Progressive delamination of laminated composites via 1D models.

Composite Structures. 2020, 235: 111799.
https://doi.org/10.1016/j.compstruct.2019.111799

[5] Moudood A, Rahman A, Khanlou HM, et al. Environmental effects on the durability and the mechanical performance of flax fiber/bio-epoxy composites. Composites Part B: Engineering. 2019, 171: 284-293.
https://doi.org/10.1016/j.compositesb.2019.05.032

[6] da Silva LFM, Adams RD. Techniques to reduce the peel stresses in adhesive joints with composites. International Journal of Adhesion and Adhesives. 2007, 27(3): 227-235.
https://doi.org/10.1016/j.ijadhadh.2006.04.001

[7] Sahu P, Mishra PC. Combine experimental and FEM analysis of adhesive bonded single lap joint with Al-alloy flat adherends and pre-embedded artificial defects. SN Applied Sciences. 2019, 1(11).
https://doi.org/10.1007/s42452-019-1535-8

[8] Monajati L, Vadean A, Boukhili R. Mechanical Behavior of Adhesively Bonded Joints Under Tensile Loading: A Synthetic Review of Configurations, Modeling, and Design Considerations. Materials. 2025, 18(15): 3557.
https://doi.org/10.3390/ma18153557

[9] Molla ST, Tsegaw AA, Bogale TM, et al. Computational analysis of stress distribution in adhesively bonded hybrid sisal-glass reinforced high-density polyethylene composite. Journal of Reinforced Plastics and Composites. Published online February 12, 2026.
https://doi.org/10.1177/07316844261419578

[10] Li C, Zhang Y, Zhang K, et al. Full-Scale Cohesive Zone Modeling and Experimental Investigation of Debonding Behaviors in Root Joints for Wind Turbine Blades. Polymer Composites. 2025, 47(3): 2301-2313.
https://doi.org/10.1002/pc.70282

[11] Špirk S, Kalina T. Validated Cohesive Zone Models for Epoxy-Based Adhesive Joints Between Steel and CFRP Composites for Multimaterial Structural Design in Transportation Applications. Polymers. 2026, 18(3): 309.
https://doi.org/10.3390/polym18030309

[12] Poodts E, Ghelli D, Brugo T, et al. Experimental characterization of a fiber metal laminate for underwater applications. Composite Structures. 2015, 129: 36-46.
https://doi.org/10.1016/j.compstruct.2015.03.046

[13] Wei K, Chen Y, Li M, et al. Strength and Failure Mechanism of Composite-Steel Adhesive Bond Single Lap Joints. Riccio A, ed. Advances in Materials Science and Engineering. 2018, 2018(1).
https://doi.org/10.1155/2018/5810180

[14] Kadioglu F, Avil E, Ercan ME, et al. Effects of different overlap lengths and composite adherend thicknesses on the performance of adhesively-bonded joints under tensile and bending loadings. IOP Conference Series: Materials Science and Engineering. 2018, 369: 012034.
https://doi.org/10.1088/1757-899x/369/1/012034

[15] Bernardin P, Sedlacek F, Kozak J, et al. Identification of the Cohesive Parameters for Modelling of Bonded Joints between Flat Composite Adherends with Thick Layer of Adhesive. Materials. 2024, 17(19): 4880.
https://doi.org/10.3390/ma17194880

[16] Liljedahl CDM, Crocombe AD, Wahab MA, et al. Damage modelling of adhesively bonded joints. International Journal of Fracture. 2006, 141(1-2): 147-161.
https://doi.org/10.1007/s10704-006-0072-9

[17] da Silva RV, Voltz H, Filho AI, et al. Hybrid composites with glass fiber and natural fibers of sisal, coir, and luffa sponge. Journal of Composite Materials. 2020, 55(5): 717-728.
https://doi.org/10.1177/0021998320957725

[18] Caglar H, Idapalapati S, Sharma M, et al. Stress Analysis of Glass Fiber-Reinforced Polymer Lap Joints with Modified Adhesives at Various Temperatures. Journal of Composites Science. 2024, 8(10): 406.
https://doi.org/10.3390/jcs8100406

[19] Yu Y, Pan Y, Zhou R, et al. Effects of Water and Alkaline Solution on Durability of Carbon-Glass Hybrid Fiber Reinforced Polymer Bars. Polymers. 2021, 13(21): 3844.
https://doi.org/10.3390/polym13213844

[20] Mendoza-Navarro LE, Diaz-Diaz A, Castañeda-Balderas R, et al. Interfacial failure in adhesive joints: Experiments and predictions. International Journal of Adhesion and Adhesives. 2013, 44: 36-47.
https://doi.org/10.1016/j.ijadhadh.2013.02.004

[21] Sun J, Zhang S, Xu L, et al. Simulation analysis method of adhesive bonding strength for steel-carbon fiber composites and its application in automotive B-pillars. Composites and Advanced Materials. 2025, 34: 26349833251392954.
https://doi.org/10.1177/2634983325139295

[22] Sane AU, Padole PM, Manjunatha CM, et al. Mixed mode cohesive zone modelling and analysis of adhesively bonded composite T-joint under pull-out load. Journal of the Brazilian Society of Mechanical Sciences and Engineering. 2018, 40(3).
https://doi.org/10.1007/s40430-018-1056-1

[23] Gesese NA, Tesfay AG. Green hybrid composites for automotive roof applications: experimental study and design optimization using reused PET and jute fiber reinforcements. Composites and Advanced Materials. 2026, 35: 26349833261425661.
https://doi.org/10.1177/2634983326142566

[24] Wu XF, Zhao Y, Zholobko O. Stress-Function Variational Method for Accurate Free-Edge Interfacial Stress Analysis of Adhesively Bonded Single-Lap Joints and Single-Sided Joints. Journal of Composites Science. 2021, 5(8): 197.
https://doi.org/10.3390/jcs5080197

[25] Neves LFR, Campilho RDSG, Sánchez-Arce IJ, et al. Numerical Modelling and Validation of Mixed-Mode Fracture Tests to Adhesive Joints Using J-Integral Concepts. Processes. 2022, 10(12): 2730.
https://doi.org/10.3390/pr10122730